一般セッション(口頭講演) | 3 光・フォトニクス：3.3 生体・医用光学（旧3.4）

2023年9月20日(水) 9:00 ~ 11:30 | A305 (熊本城ホール)

[20a-A305-1~9] 3.3 生体・医用光学（旧3.4）

南川 丈夫(徳島大)、 安野 嘉晃(筑波大)

英語発表

9:00 ~ 9:15

[20a-A305-1] Quantitative intra-tissue activity imaging technique for evaluating *in vitro* cell culture samples by optical coherence tomography

○(M2)Rion Morishita[1], Toshio Suzuki[2,3], Pradipta Mukherjee[1], Ibrahim Abd El-Sadek[1,4], Tanatchaya Seesan[5], Yiheng Lim[1], Shuichi Makita[1], Yuki Yamamoto[3], Tetsuharu Nagamoto[3], Yoshiaki Yasuno[1] (1.COG, Univ. of Tsukuba, 2.Univ. of Tsukuba, 3.HiLung Inc., 4.Damietta Univ., 5.KMITL)

英語発表

9:15 ~ 9:30

[20a-A305-2] Deep learning based high-speed three-dimensional dynamic optical coherence tomography generation for tumor spheroid evaluation

○(M2)Yusong Liu[1], Ibrahim Abd El-Sadek[1,2], Shuichi Makita[1], Tomoko Mori[3], Atsuko Furukawa[3], Satoshi Matsusaka[3], Yoshiaki Yasuno[1] (1.COG, Univ. of Tsukuba, 2.Faculty of Science, Damietta Univ., 3.Faculty of Medicine, Univ. of Tsukuba)

英語発表

9:30 ~ 9:45

[20a-A305-3] Assessing the effect of metabolic inhibitor drugs on liver functionality with dynamic optical coherence tomography

○(P)Pradipta Mukherjee[1], Donny Lukmanto[1], Shinichi Fukuda[1], Toshiharu Yamashita[1], Kosuke Okada[1], Thi Hang Tran[1], Ibrahim Abd El-Sadek[1,2], Shuichi Makita[1], Yoshiaki Yasuno[1] (1.Univ. of Tsukuba, 2.Daimetta Univ.)

英語発表

9:45 ~ 10:00

[20a-A305-4] Computational-hardware hybrid methods for tissue deep imaging in Jones matrix polarization-sensitive optical coherence tomography

○(DC)Lida Zhu[1], Shuichi Makita[1], Junya Tamaoki[2], Antonia Lichtenegger[3], Yiqiang Zhu[1], Makoto Kobayashi[2], Yoshiaki Yasuno[1] (1.Computational Optics Group, University of Tsukuba, 2.Department of Molecular and Developmental Biology, University of Tsukuba, 3.Center for Medical Physics and Biomedical Engineering, Medical University of Vienna)

英語発表

10:00 ~ 10:15

[20a-A305-5] *In vivo* dynamic optical coherence tomography with hardware- and software-based motion correction methods

○(M1)YU GUO[1], Rion Morishita[1], Ibrahim Abd El-Sadek[1,2], Pradipta Mukherjee[1], Yiqiang Zhu[1], Yoshiaki Yasuno[1] (1.Univ. of Tsukuba, 2.Damietta Univ.)

10:30 ~ 10:45

[20a-A305-6] 波長830 nm帯高分解能スペクトル領域光コヒーレンス顕微鏡（OCM）の開発

○西原 共紀[1]、西澤 典彦[1] (1.名大院工)

10:45 ~ 11:00

[20a-A305-7] バイオスペックルOCTを用いたマイクロプラスティックの濃度・粒径の植物種子への影響モニタ

○黒川 知郁[1]、Y Sanath[1]、門野 博史[1] (1.埼大理工研)

英語発表

11:00 ~ 11:15

[20a-A305-8] Application of bio-speckle on micro-bioassay with Zooplankton and phytoplankton

○(D)Devi Arti Devi[1], Hirofumi Kadono[1], Uma Maheswari Rajagopalan[2] (1.Graduate School of Science and Engineeing Saitama University, 255 shimookubo, Sakura ward, Saitama, 338-0825, Japan, 2.Department of mechanical Eng. Faculty of Engineering, Shibaura Institute of Technology, Japan)

11:15 ~ 11:30

[20a-A305-9] 円偏光散乱を用いたスキルス胃がん検出

○西沢 望[1]、島田 周[2]、田中 真二[2] (1.北里大理、2.東京医歯大)

Quantitative intra-tissue activity imaging technique for evaluating *in vitro* cell culture samples by optical coherence tomography

○Rion Morishita[1], Toshio Suzuki[2,3], Pradipta Mukherjee[1], Ibrahim Abd El-Sadek[1,4], Tanatchaya Seesan[5], Yiheng Lim[1], Shuichi Makita[1], Yuki Yamamoto[3], Tetsuharu Nagamoto[3], and Yoshiaki Yasuno[1]

Computational Optics Group, Univ. of Tsukuba[1]; Faculty of Medicine, Univ. of Tsukuba[2]; HiLung Inc.[3]; Faculty of Science, Damietta Univ.[4]; School of Science, King Mongkut's Institute of Technology Ladkragang[5]

1. Introduction

Organoid is a three-dimensional (3D) *in vitro* cell culture that mimics the structures and functions of human organs, and generally used for drug development and disease mechanism research [1]. Several imaging techniques have been used for assessing organoids [2]. However, none of these technologies can fulfill all requirements for the organoid imaging, i.e., 3D imaging, micrometer-scale resolution, millimeter-scale image depth, non-invasiveness, and sensitivity to tissue activity.

Recently, dynamic optical coherence tomography (DOCT) has been developed. DOCT analyzes the time characteristics of time-sequential OCT signals to visualize intra-tissue activity with label-free, few-μm resolution, few-mm penetration, and in 3D. Logarithmic intensity variance (LIV) is one of the DOCT contrasts that is sensitive to the magnitude of intra-tissue activity [3,4]. But LIV cannot contrast the speed of activity. In this work, we introduce a quantitative DOCT algorithm to quantify the "speed" and "magnitude" of intra-tissue activity, called variable time window LIV (VLIV). This approach has been applied to human induced pluripotent stem cell (hiPSC)-derived alveolar organoids and its fibrotic model to demonstrate the label-free tissue activity imaging.

2. Principle and study protocol

In VLIV algorithm, two quantitative metrics, named damping factor (DF) and magnitude factor (MF), are computed from time-sequential OCT data. VLIV is based on LIV computation which is time variance of logarithmic OCT intensity signals. Mean LIVs are computed for all possible time windows so that LIV is computed as a function of time window τ. The LIV time function is modeled by a first-order saturation function of

$$\mathrm{LIV}(\tau) = a\,[1 - \exp(-\tau/b)]\,, \qquad (1)$$

where a and b are the fitting parameters, τ is the time window. MF is defined as MF $\equiv a$, which is the saturation value. DF is defined as DF $\equiv 1/b$ (1/time-constant). MF and DF may be sensitive to the magnitude and speed of the tissue motility, respectively.

In this study, an 840-nm spectral domain OCT was used. The axial and lateral resolutions are 3.8 μm (in tissue) and 4.9 μm, respectively. The time-sequential OCT data are acquired with a repeating raster scan protocol [4]. Each location was scanned 32 times with a frame repetition time of 202.6 ms.

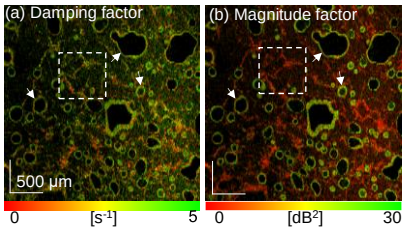

Figure 1: The DF (a), and MF (b) *en face* images of day 3 normal model. FOV is 3 × 3 mm^2.

The hiPSC-derived alveolar organoids include normal and fibrotic models [5,6]. The fibrotic model was induced by bleomycin. Hereafter, we denote the fibrotic model as "bleomycin model." Both the models were cultured for 3, 7, 10, 16, 17, and 18 days after the organoid establishment were investigated.

3. Results and discussion

DF and MF images of alveolar organoid are shown in Figs. 1 and 2. On the entire organoid, a uniform distribution of alveoli with cystic structures shows high DF (green) and high MF (green) [arrows, Fig. 1]. Fibroblasts with mesh-like structures show moderate DF (yellow) and low MF (red) [squares, Fig. 1]. Focusing on the alveoli [circles, Fig. 2], thickened epitheliums are observed. The inner surface of the epithelium shows higher DF and lower MF than the other part of the epithelium. The thickened epithelium in bleomycin model may indicate an abnormal remodeling or repairing process, such as bronchiolization [7].

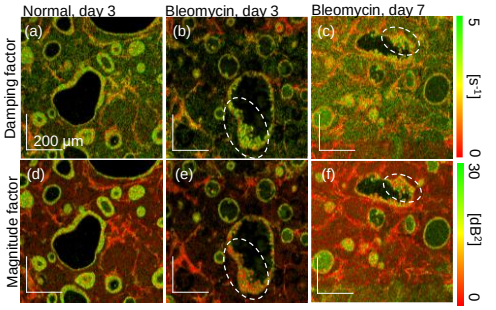

Figure 2: The DF (a-c), and MF (d-f) *en face* images focusing on alveoli. FOV is 1 × 1 mm^2.

4. Conclusion

A DOCT based method was introduced that enables quantifying the speed and magnitude of intra-tissue activity. Two quantitative metrics, MF and DF, revealed the morphological and functional structures in the alveolar organoids. Notably, MF and DF revealed an abnormal activity distribution in the alveolar epithelium of bleomycin models, associated with abnormal remodeling of the alveolar epithelium.

References

[1] Clevers, Cell **165**, 1586–1597 (2016). [2] Fei, Bioengineering **9**, 121 (2022). [3] El-Sadek, Biomed. Opt. Express **11**, 6231–6248 (2020). [4] El-Sadek, Biomed. Opt. Express **12**, 6844–6862 (2021). [5] Gotoh, Stem Cell Reports **3**, 394–403 (2014). [6] Yamamoto, Nat Methods **14**, 1097–1106 (2017). [7] Desai, Nature **507**, 190–194 (2014).

Deep learning based high-speed three-dimensional dynamic optical coherence tomography generation for tumor spheroid evaluation

○Yusong Liu[1], Ibrahim Abd El-Sadek[1,2], Shuichi Makita[1], Tomoko Mori[3], Atsuko Furukawa[3], Satoshi Matsusaka[3], Yoshiaki Yasuno[1]

Computational Optics Group, Univ. of Tsukuba[1]; Faculty of Science, Damietta Univ [2]; Faculty of Medicine, Univ. of Tsukuba[3]

E-mail: yusong.liu@cog-labs.org

1. Introduction

Cancer is a leading cause of human death. Anti-cancer drug selection becomes the key for cancer therapy. Tumor spheroid cultured from patient's originated tumor cells is useful for anti-cancer drug investigation[1]. A dynamic optical coherence tomography (D-OCT) method, logarithmic OCT intensity variance (LIV) was proposed for drug response evaluation of tumor spheroid. Three-dimensional (3-D) LIV successfully visualized and quantitatively assessed the response patterns of tumor spheroid to anti-cancer drugs[2].

However, the slow volumetric acquisition (around 52.4 s per volume) of LIV is not suitable for comprehensive drug response analysis with large numbers of samples. In this study, we proposed a deep-learning-based method that requires short acquisition time to achieve high-speed 3-D LIV generation for tumor spheroid evaluation.

2. Method

Conventional 3-D LIV was obtained from 32 OCT frames within 6.348-s time window by conventional algorithm[2], and here denoted as C32LIV. A U-shape[3] neural network (NN) model was trained based on image pairs of four OCT frames within 4.92-s time window as input and C32LIV as ground truth. The four OCT frames were the 8th, 16th, 24th, 32nd frames extracted from the thirty-two frames which were used for C32LIV computation. Here the LIV generated from four OCT frames within 4.92-s time window by NN was denoted as NN4LIV. The training data set consists of 41,928 image pairs from thirty-six human breast (MCF-7 cell line) and twenty-four colon (HT-29 cell line) tumor spheroids. The NN-based LIV generation algorithm reduces the required 3-D acquisition time from 52.4 s to 6.55 s.

Trained NN model was evaluated based on twelve MCF-7 and twelve HT-29 tumor spheroids. Besides C32LIV and NN4LIV, we also computed the LIV from the four OCT frames same as those used for NN4LIV by conventional algorithm and denoted it as C4LIV. We compared NN4LIV and C4LIV with C32LIV based on image appearance and numerical metrics, namely volume-wise mean LIV and volume-wise viable cell ratio. The viable cell ratio is defined as the number of pixels in spheroid with higher LIV than 3dB² divided by number of entire spheroid pixel number.

3. Results

Figure 1 represents the cross-sectional and *en-face* images of C32LIV, NN4LIV, and C4LIV of MCF-7 spheroid treated with 1-μM of paclitaxel. High and low LIV signals may indicate viable and necrotic cells, respectively[2]. C32LIV and NN4LIV have consistent appearance: low LIV signals at spheroid core and high LIV signals at spheroid periphery. However, C4LIV shows more low LIV signals at the periphery region. Figure 2 shows (a) mean LIV and (b) viable cell ratio at the entire spheroid volume. The ideal line indicated metrics of C32LIV. The metrics of NN4LIV are close to that of C32LIV. In contrast, C4LIV has a large difference especially in the high-LIV and high-viable-cell-ratio cases.

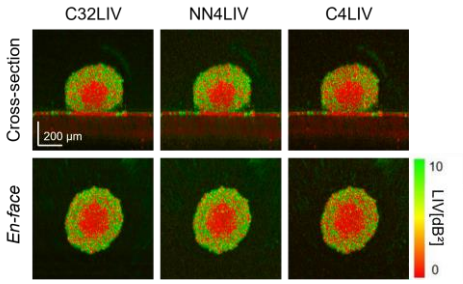

Figure 1: Cross-sectional and *en-face* images of C32LIV, NN4LIV, and C4LIV of 1-μM paclitaxel treated MCF-7 tumor spheroid.

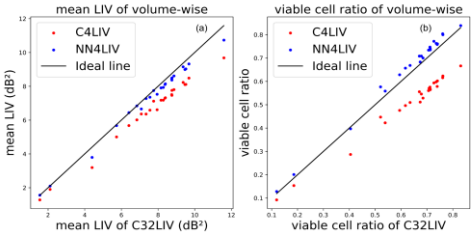

Figure 2: Plots of (a) volume-wise mean LIV and (b) volume-wise viable cell ratio of C32LIV, NN4LIV, and C4LIV.

4. Conclusion

We used a NN model to generate 3-D LIV that requires around 6.55 s for a volumetric acquisition, which is only 12.5% of that of conventional algorithm. Our NN-based LIV algorithm has potential for high-speed three-dimensional LIV generation and replacing C32LIV for three-dimensional evaluation of tumor spheroid.

Reference

[1] B. Galateanu, International Journal of Oncology **48**(6), 2295–2302 (2016). [2] I. A. El-Sadek, Biomed. Opt. Express **12**(11), 6844 (2021). [3] O. Ronneberger, (2015)

Assessing the effect of metabolic inhibitor drugs on liver functionality with dynamic optical coherence tomography

University of Tsukuba[1], Damietta University[2], °Pradipta Mukherjee[1], Donny Lukmanto[1], Shinichi Fukuda[1], Toshiharu Yamashita[1], Kosuke Okada[1], Thi Hang Tran[1], Ibrahim Abd El-sadek[1,2], Shuichi Makita[1], and Yoshiaki Yasuno[1]

E-mail: pradipta.mukherjee@cog-labs.org

We present label-free imaging of the functional activity of liver tissue in the presence of metabolic inhibitor drugs using dynamic optical coherence tomography (DOCT). We observed a structural correlation between the early time point DOCT and the late time point OCT, as well as changes in tissue functionality over time.

1. Introduction

The liver is divided into three distinct functional zones: the periportal, pericentral, and intermediate zones, based on their metabolic activity [1]. The periportal zone involves in gluconeogenesis, while the pericentral zone specializes in the glycolysis process. Visualizing the functional activity of these zones in all three dimensions (3D) without any labeling agents is important for identifying and assessing liver injuries during liver diseases.

To selectively target specific metabolic pathways within the different functional zones of the liver, metabolic inhibitor drugs can be used. For example, 2-deoxyglucose (2-DG) can inhibit glycolysis, which predominantly occurs in the pericentral zone of the liver [2].

Dynamic optical coherence tomography (DOCT) has recently emerged as a technique that allows for imaging tissue function without the need for labeling agents [3]. In this study, we present 3D functional activity imaging of liver tissue in the presence of metabolic inhibitor drugs using DOCT.

2. Method and measurement protocol

We used C57BL/6 mice for our experiment. A direct injection of 200 µL/kg body weight of the 2-deoxyglucose (2-DG) drug was administered to the liver. After sacrificing the mice, the livers were extracted and immersed in a PBS solution. To observe and track changes in liver function over time, longitudinal time-course OCT measurements were taken at the same location every 30 minutes for a duration of 10 hours. This study utilized a custom-built swept-source OCT system [4], with a central wavelength of the light source at 1.3 µm and a scanning speed of 50,000 A-lines/s. To obtain 3D DOCT images, a combination of a repeating raster scan protocol [5] and a signal processing algorithm called logarithmic intensity variance (LIV) was employed. In the repeating raster scanning protocol, 16 frames were captured at each B-scan location of the sample, with a frame repeating time of 204.8 ms. The total volume acquisition time for 128 locations in the sample was 26.2 seconds. The LIV contrast was calculated by computing the temporal variance of the logarithmic (dB)-scale OCT intensity among the repeated frames at each B-scan location [3].

3. Results

Figure 1 represents *en face* projection (first row) and cross-sectional (second row) OCT and LIV images at the initial (2.5-hr) and late (9.5-hr) time points. At deeper depths, three-dimensional vessel-like structures can be observed in the depth color-coded LIV projection (b), and these structures diminish over time (d). By comparing the 2.5-hr depth color-coded LIV image and the 9.5-hr maximum OCT projection, structural correlations can be identified in the region marked by the rectangles in (b) and (c). It appears that the tissue showing high LIV at the 2.5-hr time point becomes hyper scattering at the 9.5-hr time point. The same hyperscattering appearance can also be observed in the OCT cross-section [arrowhead (f)]. Such appearance may suggest that the glycolysis process in the liver is inhibited by 2-DG, resulting in gradual necrosis of the pericentral tissue. This necrosis causes a decrease in LIV and also leads to hyperscattering in OCT image.

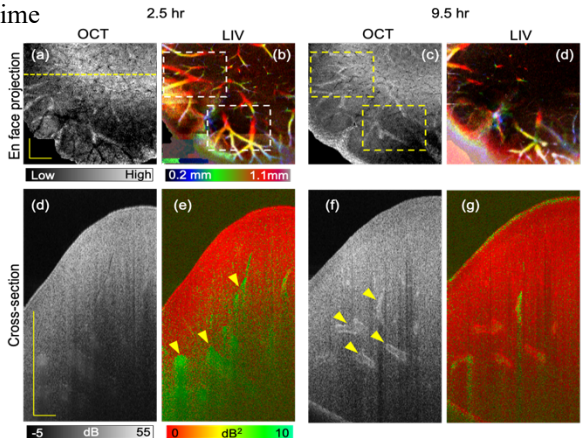

Fig.1: liver functionality imaging after drug injection.

4. Conclusion

The 3D vessel-like metabolic structures within the liver, which likely correspond to its functional zone's activity was observed using DOCT. The observed LIV reduction in these structures and the emergence of hyperscattering structures may indicate a loss of functionality and the appearance of necrotic tissue over time. In conclusion, DOCT imaging can be used as an assessment tool to investigate the drug effect on liver functional zones activity.

References:

1) Gebhardt et al., World J. Gastroenterol. 20, 8491–8504 (2014). 2) Wang et al., Molecular Medicine Reports 11, 1917– 1924 (2015). 3) El-Sadek et al., Biomed. Opt. Express **11**, 6231–6248 (2020). 4) Li et al., Biomed. Opt. Express **8**, 1290–1305 (2017). 5) El-Sadek et al., Biomed. Opt. Express **12**, 6844–6863 (2021).

Computational-hardware hybrid methods for tissue deep imaging in Jones matrix polarization-sensitive optical coherence tomography

◦Lida Zhu[1], Shuichi Makita[1], Junya Tamaoki[2], Antonia Lichtenegger[3], Yiqiang Zhu[1], Makoto Kobayashi[2], and Yoshiaki Yasuno[1]

COG, University of Tsukuba [1]; Department of Molecular and Developmental Biology, University of Tsukuba[2]; Center for Medical Physics and Biomedical Engineering, Medical University of Vienna[3]

E-mail: lida.zhu@cog-labs.org

1. Background

Recent progress in tissue culture techniques has facilitated the cultivation of thick and functionally-shaped tissues in basic medical researches [1]. Imaging such thick tissue cultures presents several challenging requirements: high resolution of a few microns, deep imaging depth of a few millimeters, and intrinsic molecular contrast of specific tissues.

Recently, polarization-sensitive optical coherence tomography (PS-OCT) has attracted attentions from the biomedical researchers. PS-OCT is a non-invasive label-free imaging modality that potentially it fulfills these requirements. However, deep imaging with PS-OCT in tissue still faces several challenges: the trade-off between lateral resolution and depth-of-focus (DOF), and the multiple-scattering (MS) signal that appears in the deep regions, which degrades the image contrast.

2. Method

We developed new computational-hardware-hybrid methods to address these two challenges in deep imaging using our custom-build Jones matrix PS-OCT (JM-OCT) [2]. The computational approach, named computational refocusing [3], removes the trade-off between lateral resolution and DOF. The hybrid approach, named multi-focus averaging (MFA) [4], combines computational refocusing, complex averaging, and an electrical tunable lens (ETL). It averages multiple refocused Jones matrices of PS-OCT signals acquired with different focus configurations (7 volumetric Jones matrices acquired with different focus depth positions, with an interval of 0.12 mm between each depth position) to reduce the MS signal and enhance image contrast in deep regions.

3. Results

Figure 1 shows the 3-D cut-away intensity images of an *ex vivo* porcine muscle without and with applying refocusing. The focus was located at a depth around 1 mm. In the deep region (1.06 mm), the resolution improvement obtained with the refocusing is moderate. However, at superficial depths (0 mm and 0.38 mm) the resolution is noticeably improved by the refocusing, and muscle fiber structures can be clearly visualized.

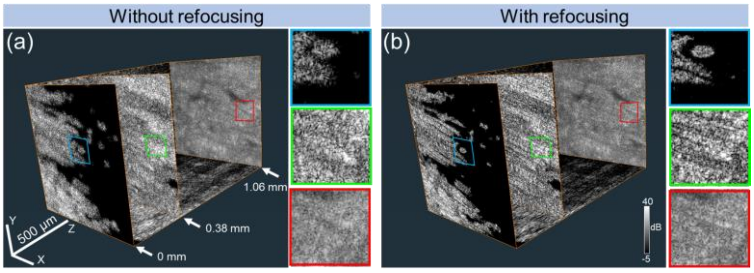

Figure 1. Three-dimensional cut-aways of intensity images of an *ex vivo* porcine muscle without (a) and with (b) applying computational refocusing.

Figure 2 compares the intensity and birefringence images of a postmortem adult medaka fish obtained by the MFA and single acquisition methods. Tissue birefringence can be caused by fibrous structure such as muscle and collagen. In the intensity images, the MFA provides better contrast for some low-scattering structures [white arrows in Figs. 2(a, c, e, g)]. In the birefringence images, the MFA images show low birefringence (blue appearance) of skin in the deep regions [yellow arrows in Figs. 2(b, d, f, h)]. The birefringence contrast between the skin and neighboring muscle regions is enhanced by applying MFA method.

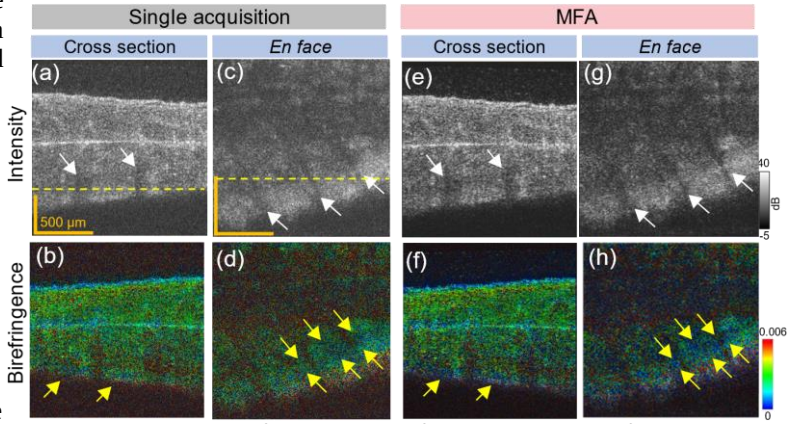

Figure 2. Intensity and birefringence images of a postmortem medaka fish measured by single acquisition and MFA methods. Yellow dashed lines indicate the locations where the cross section and *en face* images are taken.

4. Conclusion

Our computational-hardware-hybrid methods successfully achieve high resolutions throughout the imaging depth, reduce the MS signals and enhance the image contrast in the deep regions. This work has important implications for polarization-sensitive imaging of thick biological tissues, empowering PS-OCT as a more practical tissue imaging modality.

References

[1] R.-Z. Lin et al. Biotechnol. J. 3, 1172–1184 (2008). [2] A. Miyazawa et al. Biomed. Opt. Express 10, 5162–5181 (2019). [3] L. Zhu et al. Biomed. Opt. Express 13, 2975–2994 (2022). [4] L. Zhu, et al. arXiv:2304.11309 (2023).

In vivo dynamic optical coherence tomography with hardware- and software-based motion correction methods

○Yu Guo[1], Rion Morishita[1], Ibrahim Abd El-Sadek[1,2], Pradipta Mukherjee[1], Yiqiang Zhu[1], and Yoshiaki Yasuno[1]

Computational Optics Group, Univ. of Tsukuba[1], Faculty of Science, Damietta Univ.[2]

E-mail: yu.guo@cog-labs.org

1. Introduction:

Optical coherence tomography (OCT) is a non-invasive imaging modality that can provide three-dimensional (3D), high resolution, and few mm depth imaging of biological tissues. Recently, dynamic optical coherence tomography (D-OCT) has been developed to visualize and quantitatively assess the intracellular motility by statically analyzing the temporal characteristics of a-few-second sequentially captured OCT frames at the same location in the tissue [1]. However, *in vivo* D-OCT imaging is challenging due to the involuntary motions, which cause motion artifacts in D-OCT images.

In this study, we demonstrated in vivo D-OCT by employing hardware and software methods for motion correction. Using the proposed approach, *in vivo* D-OCT imaging of human skin was successfully obtained.

2. Method:

In *in vivo* sample measurement, we implemented two methods to capture a motion-suppressed D-OCT data. First is a fixation spacer to reduce involuntary motion during measurement. The fixation spacer is shown in Fig. 1 and was designed by us and printed by 3-D printer to press the sample. Second is a software-based motion correction to remove bulk motions from acquired data before D-OCT computation. The bulk motion correction algorithm registers the time sequential frames measured at the same location, then detects and corrects the bulk motion among frames along the depth- and slow-scan-direction [2].

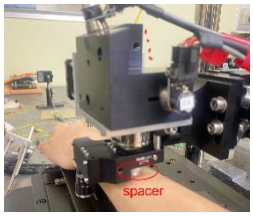

Figure 1: The photo of the fixation spacer

We measured skin of human outer forearm for *in vivo* D-OCT imaging. As D-OCT contrast, logarithmic intensity variance (LIV) was used to visualize the tissue dynamics. LIV is defined as time variance of the time sequential logarithmic OCT intensity signals [3].

To calculate the LIV, we applied the 3D dynamic scanning protocol [1] using a polarization-sensitive Jones matrix swept-source OCT system. The 3 × 3 mm2 scanning area was divided into 8 blocks and each block consist of 16 locations. Each block is imaged by a rapid raster scanning pattern and it is repeated 32 times in 6.55 s. So, 32 frames were obtained at each location with a frame repeating time of 204.8 s. The OCT volume was measured in 52.4 s.

3. Result

Figure 2 shows the LIV images of the *in vivo* human outer forearm skin. Overall, a significant reduction of the LIV signal in the entire field of view (FOV) after using the fixation spacer [Fig.2 (b)] and several vessels-like structures with high LIV were clearly observed. We believe that the high LIV signals without the spacer [Fig. 2 (a)] are a motion artifact and it is suppressed after the fixation. After applying motion correction, a better LIV image with a reduction of high LIV artifacts was observed [Fig. 2 (d)] (See the zoomed up images at the insets).

The 30 × 30-pixels area [squares, Fig. 2] below the skin surface was selected as the region of interests (ROIs). The mean LIV of the ROIs in Fig. 1(a-d) were 15.04, 5.55, 10.91, 4.98, respectively.

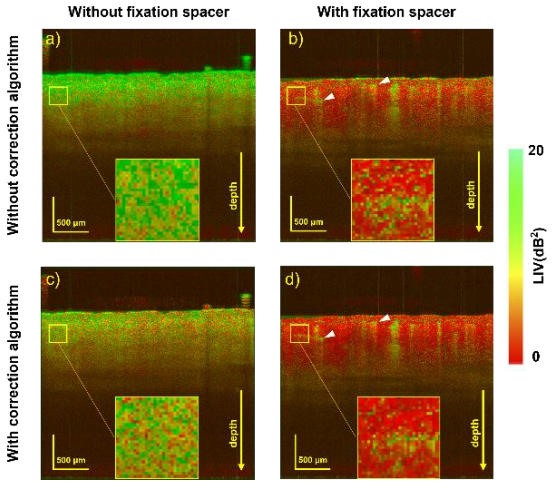

Figure 2 : B-scan LIV image of outer forearm skin. FOV is 3 × 3 mm^2.

4. Summary and conclusion:

We proposed *in vivo* D-OCT imaging of human skin using a combination of hardware- and software-based motion correction methods. A significant improvement of the D-OCT contrast was obtained and serval vessel-like structures [triangles, Fig. 2 (b), (d)], which were muddled in high LIV artifacts without using our methods, has been clearly visualized. The results indicate that our proposed methods are promising methods for *in vivo* D-OCT imaging.

References:

[1] I. A. El-Sadek et al., Biomed. Opt. Express, 12, 6844-6863 (2021). [2] R. Morishita et al., Biomed Opt. Express, 14, 2333-2351 (2023). [3] I. A. El-Sadek et al., Biomed. Opt. Express 11, 6231-6248 (2020).

波長 830 nm 帯高分解能スペクトル領域光コヒーレンス顕微鏡（OCM）の開発

Development of spectral domain optical coherence microscopy (OCM) at 830 nm wavelength

名大院工 [1] ○西原 共紀 [1]，西澤 典彦 [1]

Nagoya Univ. [1], ○Tomoki Saibara[1], Norihiko Nishizawa[1]

E-mail: saibara.tomoki.u1@s.mail.nagoya-u.ac.jp

１．はじめに

OCM（Optical Coherence Microscopy）とは、広帯域光を利用することで生体等の内部構造を非接触・非破壊でかつ、高分解能で撮影できる OCT（Optical Coherence Tomography）と共焦点顕微鏡技術を組み合わせたイメージング技術であり、OCT よりも高い横方向分解能を持つという特徴がある。今回は波長 830 nm 帯スペクトル領域 OCM を開発したので報告する。

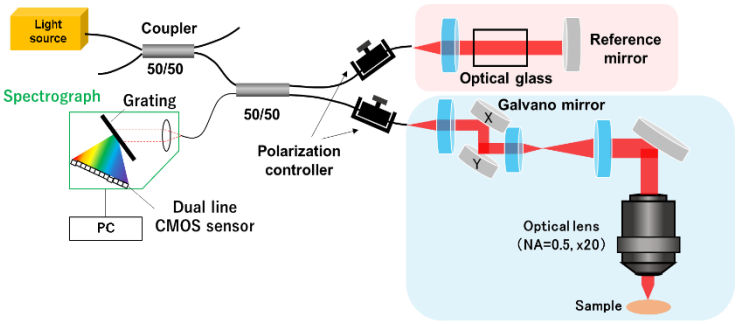

Fig 1. Experimental setup of spectral-domain OCM at 830 nm wavelength

２．原理・結果

開発したシステムの構成を Fig. 1 に示す。光源から出射された光を、カプラを用いリファレンスミラー側とサンプル側に分けて照射する。それぞれからの反射光を再びカプラで干渉させ、その干渉信号の深さ方向の強度情報を得ることにより、内部構造を撮影することができる。これまで本研究室では、同波長帯の時間領域 OCM を開発してきたが、1B スキャン画像取得時間が 2 秒程度かかってしまうという問題点があった。そこで、本研究では、時間領域 OCM で取り入れられている方式の代わりに、得られた信号を回折格子などを用いて分光し、光スペクトルをフーリエ変換する方式であるスペクトル領域 OCM を開発することにより、1B スキャン画像取得時間 0.07 秒という高速な画像取得を可能にした。

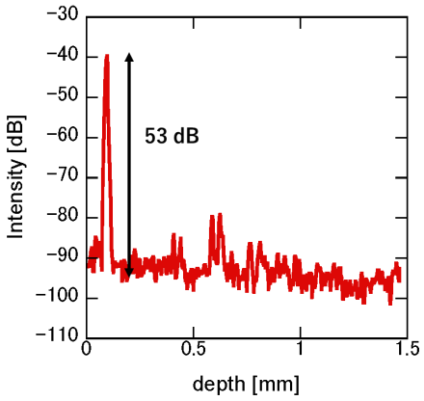

Fig 2. Interference signal

Fig. 2 に示す感度は 93 dB（減衰フィルタ 40 dB 分含む）、深さ方向分解能は 6.0 μm、横方向分解能は 1.7 μm と測定された。この OCM を用いて、直径 3 μm のビーズの XY エンフェイス画像とパイナップルの XY エンフェイス画像を取得した。その結果を Fig. 3 に示す。前者では細かい粒形を、後者では細胞壁やその内部にある微小構造まで確認することができるなど、リアルタイムで高分解能なイメージングを行うことができた。

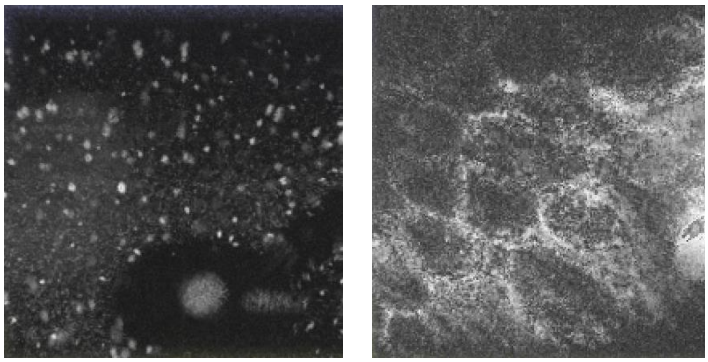

Fig 3. OCM images
(left: XY beads image, right: XY pineapple image)

バイオスペックル OCT を用いた マイクロプラスティックの濃度・粒径の植物種子への影響モニタ

Monitoring the effects of microplastic concentration and particle size on plant seeds using biospeckle OCT

埼玉大学，○(M2)黒川　知郁，Y. Sanath, 門野 博史

Saitama Univ., ○Tomofumi Kurokawa, Hirofumi Kadono

E-mail:t.kurokawa.135@ms.saitama-u.ac.jp

1. はじめに　現在マイクロプラスティックが海洋汚染や土壌汚染として社会的問題となっている.農業で多用されるプラスチック材料や,微生物や酵素によって分解される生分解性プラスチックは分解過程で,小さな微粒子に分解される.このように生じた特に,マイクロプラスティック(MP)による土壌汚染が,植物の生育に深刻な影響を与えていることが指摘されている.そこで,我々はこの問題に注目し,植物の生育に与える影響を測定するための手法を開発している.廃プラスチックは,自然の力で MP（直径 5 mm 未満）やナノプラスチック（直径 100 nm 未満）に分解され,環境中に広く拡散している[1].これまでに、MP が種子の発芽や植物の成長に悪影響を及ぼすことが報告されている[2].そこで本研究では,MP の大きさ,および濃度が植物の成長や種子の発芽に与える影響に関して,我々が独自に開発したバイオスペックル光断層画像法（bOCT）を用いてモニタリングした.

2. 実験方法　Fig. 1 に実験に用いた bOCT システムを示す．このシステムは,生物体の内部活動の変化を視覚化する非接触・非破壊の生体内モニタリング技術である[3].bOCT では,取得した OCT の断層画像から,各画素において時間軸上でスキャンの総時間にわたる画素の平均値,<I>,に対する<I>/σ_Iの標準偏差,σ_I,の比として定義されるバイオスペックルコントラストγを算出した.γの値が大きいほど組織の活性が高いことを意味する.

$$\gamma = \sigma_I / \langle I \rangle$$

濃度効果に関する実験では,コントロール,粒径 1~4 μm の MP の濃度を 5,10,15mg/L を準備した.各サンプルについて、9cm のペトリ皿のろ紙上に 6 個の種子を置いた.その後,温度 27℃,相対湿度 70%以上,照度 4000 ルクスの室内にペトリ皿を保管した.bOCT 観察は 6 時間,24 時間後におこなった.bOCT 画像の平均的なコントラストを算出し,Fig.2 に示した.次に,サイズ効果に関して実験では,コントロール,粒径 1~4 μm,10~20 μm,600~710 μm の MP を準備した.bOCT の観察は 6,12,24 時間後と測定回数を増やし,bOCT 画像の平均的なコントラストを算出し,Fig.3 に示した.

3. 実験結果・考察　濃度効果に関しては,濃度が高ければ高いほどバイオスペックルコントラスト(散乱光の強度変動を解析し,生体試料の動的な変化や活動を評価するもの)が下がっている.コントロールと MP 濃度 15mg/L では,8%もバイオスペックルコントラストの数値が減少した.このことから,MP は濃度が高ければ高いほど植物の栄養の吸収を阻害する効果が高まると考えられる.また,サイズ効果に関しては,粒径が 600~710 μm よりさらに小さい粒子の方がバイオスペックルコントラストが低く,MP による影響をより強く受けていることが分かる.これは植物が水分や栄養を吸収する際に,非常に小さい MP は表面のポアを通して植物内部に入り,組織の代謝を阻害するためであると考えられる.逆に大きな粒径の場合は,ポアをふさぐことによりで水分や栄養の吸収の阻害が生じる.そのため MP の大きさにより植物への影響の差が生じると考えられている.

【4. まとめ】　本研究では,MP の濃度効果,サイズ効果による種子の発芽をモニタするために bOCT を提案した.その結果,MP の濃度が高ければ高いほど植物の活性度が下がり,粒径は小さければ小さいほど植物の活性度は下がった.これらのことから,MP は植物に悪影響を及ぼすことが分かり,提案手法は発芽前の早い段階で MP による影響を観察することができたと考えられる.

Fig.1

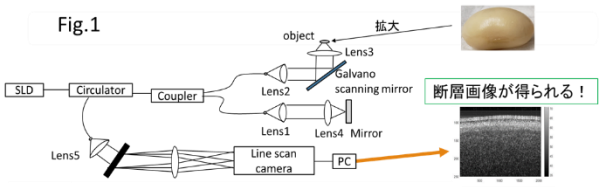

(1)Schematic diagram of the bOCT experimental system
(2) bOCT contrast after 6, 12 and 24 hours of concentration effect experiments
(3) bOCT contrast after 6, 12 and 24 hours of size effect experiments

Fig.2

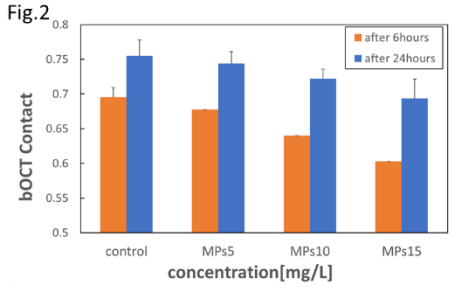

Fig.3

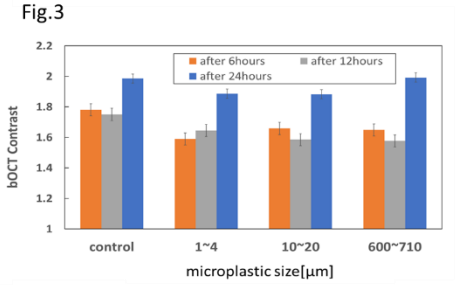

[1] H.A. Nel and P.W. Froneman, Marine Pollution Bulletin. 2015.[2] Y.S.K. De Silva, U. M. Rajagopalan, H. Kadono, GJESM. 2021.[3] Y.S.K. De Silva, U. M. Rajagopalan, H. Kadono, JSAP 2022 Spring Meeting.

Application of bio-speckle on micro-bioassay with zooplankton and phytoplankton

Devi Arti 1, Hirofumi Kadono1*, R. Uma Maheswari2

[1] Graduate School of Science and Engineering, Saitama University, Japan; [2] Dept. Mech, Eng. Faculty of Engineering. Shibaura Institute of Technology, Japan

1. Introduction

Iron (Fe) is indeed one of the most abundant heavy metals in the Earth's crust, and it can become toxic at high concentration. The main sources of iron pollution include industrial activities, transportation emissions, mining and excavation, coal combustion, and improper waste. For water pollution, recently, a micro bioassay is getting attention to quickly evaluate the toxicity of aquatic environment with very low cost without specifying chemical components. Earlier, we proposed a new technique of Biospeckle micro-bioassay, where a change of biospeckle is focused to monitor the motor ability of plankton in response to the toxicity of environment. Our previous study successfully validated its efficacy using Paramecium Chilomonas exposed to varying concentrations of the environmental toxin Zn.

In this study, we utilized Euglena and Paramecium, which has motor ability, and investigated the effects of different concentrations of the heavy metal of Fe.

2. Experiments and results

Figure 2(a) shows the experimental system where a laser diode of wavelength 638 nm was used as a light source. The sample cell of thickness 1 mm was illuminated with a diameter of 15mm. The unscattered light, or specular component, from the object was removed by a spatial filter placed at the focal plane of lens L2, and then the movement of biospeckle pattern was captured by CCD camera with 60 fps.

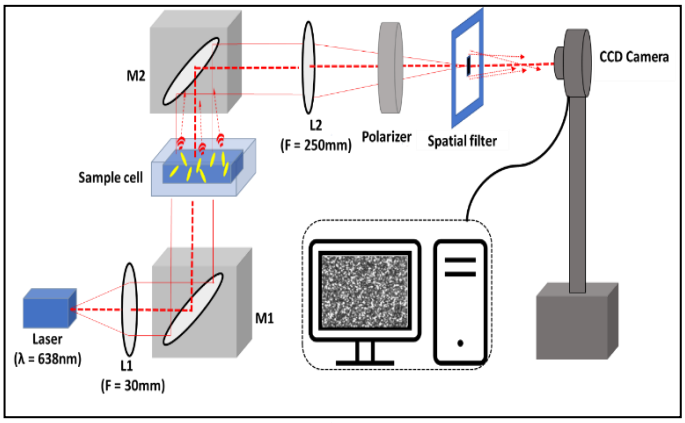

Fig.2(a). Schematic diagram of the experimental system

In this experiment, Euglena whose size was around 35-50µm was cultivated at an optimum temperature of 25°C. Their swimming activity was evaluated as a function of Fe concentration. The exposure time of Fe for each sample was 1.5 hours. To quantitatively evaluate the swimming activity of Euglena and P.chilomonas, the cross-correlation functions between the initial frame as a reference and the following frames were measured. Plankton were exposed to various concentrations of an emerging water pollutant, (FeSo4.7H2O), ranging from the permissible level (PL) of 0.1 mg/L (WHO), to 2× (0.2mg/L), 10× (1mg/L), and 20× (2mg/L) the PL. The experimental results revealed that the cross-correlation time for P. Chilomonas (shown in Fig. 2b) was smaller at a concentration of 2× the permissible level compared to the control, indicating that (FeSo4.7H2O) acts as a micronutrient for P. Chilomonas. However, as the concentration increased from the permissible level to 10× and 20× the permissible level, a significant increase in the correlation time was observed. This suggests that concentrations above 2× the permissible level were found to be toxic to P. Chilomonas. These findings indicate that P. Chilomonas is more sensitive to water toxicity. Interestingly, in contrast to P. Chilomonas, no significant change in the cross-correlation time was observed when the concentration of Euglena was increased up to 2×PL. This suggests that Euglena has a higher tolerance to the pollutant. However, with further increments in the concentration of Fe, specifically at 200× the PL (20mg/L), 500× the PL (50mg/l), and 1000× the PL (100mg/L), a clear trend emerged. As the concentration increased beyond the 200× PL, a significant increase in the correlation time was observed, indicating water toxicity. The results reveal contrasting sensitivities of P. Chilomonas and Euglena to the pollutant (FeSo4.7H2O). P. Chilomonas is highly sensitive, while Euglena demonstrates higher tolerance. For our system, we should choose the more sensitive organisms.

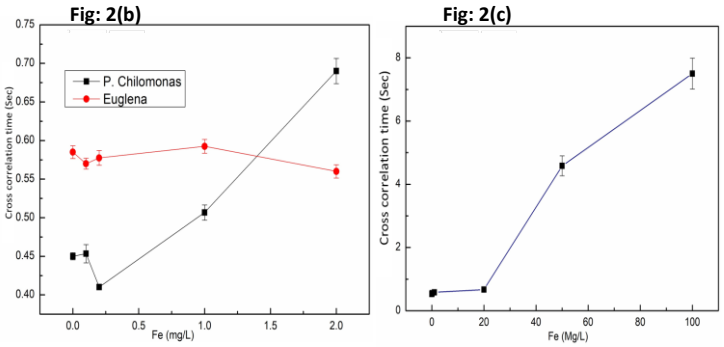

Fig 2: 2 (b) Cross-correlation length of Euglena and P.Chilomonas 2(c) Correlation time as a function of Fe concentration (mg/L) for Euglena at higher concentration.

3. Conclusion

It was confirmed that the swimming activity of microorganisms can be quantitatively evaluated by converting the image of plankton into a biospeckle image using the cross-correlation function. Several factors suggest our method could be used to assess the toxicity of an environment quickly, such as avoiding microscope observation to obtain critical features of targeted plankton such as alive/dead, as organisms become smaller, observation becomes harder due to the narrow focal depth of the imaging system.

[2] [20a-C301-8], Application of bio-speckle on micro bioassay with plankton III

円偏光散乱を用いたスキルス胃がん検出

Scirrhous gastric cancer detection using scattering of circularly polarized light

北里大理[1]，東京医科歯科大[2] ○西沢 望[1]，島田 周[2]，田中 真二[2]

Kitasato Univ.[1], Tokyo Medical and Dental Univ.[2], ○N. Nishizawa[1], S. Shimada[2], S. Tanaka[2]

E-mail: nishizawa.nozomi@kitasato-u.ac.jp

スキルス胃がんは、がん細胞が粘膜下に広く浸潤し、転移が著しいがんであり、また術後再発が多く抗癌剤耐性も強いため予後の悪い難治性がんである。さらに初期段階では、がん細胞が散在する（未分化型）ため胃壁に明確な病変が見られないことが多く早期発見が難しい[1]。そのため、スキルス胃がんの早期発見する手法が求められている。一方、我々は円偏光を生体組織に照射し、その散乱光の偏光状態の変化によりがんを検出、評価する技術の開発を進めており、これまで早期がんの深達度計測の実証などを報告してきた[2]。この技術では、散乱領域である直径 2 mm 程度、深さ 3 mm 程度の領域中のがん化に起因した細胞核異型を検出することで表面から進行しているがんの深達度を計測することができる。同様に、未分化型がんである場合にも散乱光の偏光度変化として領域内の細胞核異型の存在を検出することができる。すなわち初期スキルス胃がんを検出することが可能である。これまでにシミュレーションにより組織内のがん細胞の存在比率に応じて散乱光の円偏光度が変化することを報告した[3]。本研究では、スキルス胃がんマウスモデルから摘出した胃検体に対して実験的に検出が可能か検証したので報告する。

スキルス胃がんマウスモデルから摘出した胃検体[4]および正常な胃検体に対して Fig.1(a)に示すように右回り円偏光(DOCP = +1)を垂直に照射し、30°方向に散乱した光の偏光度を計測した。がん細胞検出に最適化した 600nm および 950nm の 2 つ波長の円偏光[2]を照射し、それらの偏光度の差分を計測した。結果を Fig.2 に示す。正常胃検体では 8mm 角の領域においてほぼ均一な値が得られ、細胞核異型が見られない。一方で、スキルス胃がん検体では腸上皮化生が表面にありがん細胞が深部に分散している 5mm 角の領域（Fig.1(b)の白点線領域）に対して測定したところ、$X = 0\sim2\ (mm), Y = 0.5\sim2.5(mm)$の領域において周辺部と大きく異なる偏光度差が得られ、スキルス胃がんの分布に対応する結果が得られた。測定により推定された部位について現在、詳細な組織分析を行っており、当日はより詳細な測定結果との対応関係を報告する予定である。

[1] Japanese Gastric Cancer Association, Gastric Cancer. **1**, 10-24 (1998). [2] N. Nishizawa *et al.*, 70th JSAP Spring Meeting, 15a-A405-6 (2023). [3] N. Nishizawa *et al.*, 69th JSAP Spring Meeting, 25p-P08-3 (2022). [4] S. Shimada *et al*., Gut. **61**, 344-353 (2012). [5] N. Nishizawa *et al*., J. Biophotonics, **15**(10), 202200062.(2021).

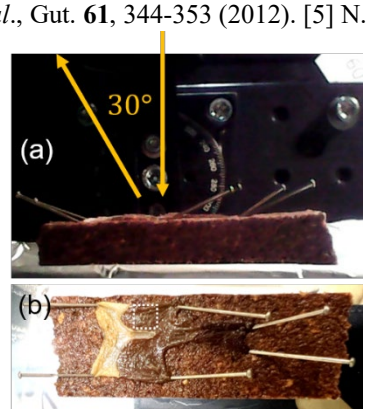

Fig. 1: Photos of the mouse stomach with scirrhous gastric cancer: (a) Side view with orange arrows which schematically show the incident and scattered light. (b) Top view with a white dotted square which indicates scan area in this study.

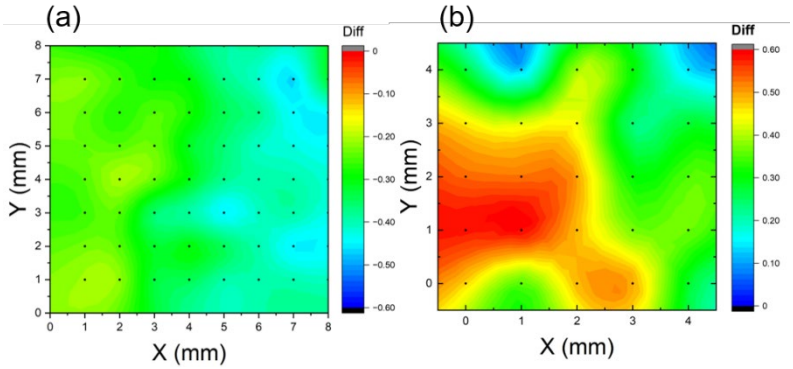

Fig. 2: Distributions of the differences in DOCP values between 600 nm and 950 nm for (a) normal stomach and (b) scirrhous gastric cancer are shown in color map. The widths of the color scale are the same, while the absolute values are different. Black points in the plotted area represent the sampling points.